Nanotechnology **21** (2010) 105203 (7pp) doi:10.1088/0957-4484/21/10/105203

Hybrid solar cells based on single-walled carbon nanotubes/Si heterojunctions

Pang-Leen Ong[1], William B Euler[2] and Igor A Levitsky[1,2]

[1] Emitech, Inc, Fall River, MA 02720, USA
[2] Department of Chemistry, University of Rhode Island, Kingston, RI 02881, USA

E-mail: ilevitsky@chm.uri.edu

Received 21 October 2009, in final form 14 January 2010
Published 16 February 2010
Online at stacks.iop.org/Nano/21/105203

Abstract

Photovoltaic devices based on single-walled carbon nanotubes (SWNTs) and n-silicon heterojunctions have been fabricated by a spray deposition process. We provide direct evidence that nanotubes serve as an active photosensing material involved directly in the photon absorption process as well as contributing to charge separation, transport and collection. The characteristic band of the SWNT band in the photoconductivity spectrum matches the S_{11} absorption band of semiconducting SWNTs of 7,6 chirality. Centrifugation of the SWNTs provides two fractions. The sediment fraction exhibits a conversion efficiency (∼1.7%) higher by a factor of eight compared to the supernatant fraction. SEM images and conductivity measurements show that the SWNT network morphology of the sediment fraction has longer and thicker nanotube bundles forming highly porous films, accounting for the enhanced conductivity and higher transparency.

(Some figures in this article are in colour only in the electronic version)

1. Introduction

For the past decade, the remarkable optoelectronic properties of carbon nanotubes (CNTs) for photovoltaic (PV) applications has induced a great deal of interest in the development of new generations of organic and hybrid solar cells. However, the use of CNTs as a conductive component of CNT-conjugated polymer composites has so far demonstrated low conversion efficiency (∼1%) despite extensive exploration of various types of nanotubes and polymers [1–7]. Another way to employ CNTs in solar cell design is the use of CNTs as a transparent conductive coating to replace metal oxide electrodes (e.g. ITO) for organic photovoltaics [8, 9]. Nevertheless, little progress has been achieved in this direction as the conductivity of the CNT network is still lower than the conductivity of ITO at the same transparency level in the visible spectral range.

Very recently, several groups reported hybrid PVs based on a CNT/n-type Si heterojunction [10–12]. A major benefit of such an approach is the combination of charge separation at the CNT/Si interface along with charge transport and collection. Thus, CNT films work not only as a transparent electrode but also as an active photosensing material. Because semiconducting single-walled nanotubes (SWNTs) and double-walled nanotubes (DWNTs) are naturally p-type conductors, when interfaced with n-type Si, they form p–n heterojunctions, exhibiting typical diode I–V characteristics. Photoconversion of such devices is mostly dictated by strong light absorption by Si for photon energies higher than the Si bandgap (1.1 eV), followed by charge separation at the SWNT/Si interface. The contribution of SWNTs' and DWNTs' light absorption to the solar cell conversion efficiency was not clear in the earlier studies [10–12]. Meanwhile, semiconducting SWNTs and DWNTs are strong light absorbers in the visible and NIR range, and that could bring additional advantages over other organic PV materials, in which light absorption is mainly limited to the NIR range.

In this study, we demonstrate that SWNT light absorption in the NIR range indeed contributes to the photoconversion process of an SWNT/n-Si solar cell. Photogenerated excitons in SWNTs dissociate into holes and electrons at the heterojunction followed by hole transport and collection through the SWNT network. In parallel, photoelectrons generated at the Si side diffuse from the depletion region to the external electrode. Thus, the SWNT film should be thick enough to absorb incident NIR light (photon energies less than 1.1 eV) but, at the same time, sufficiently thin to transmit light (photon energies more than 1.1 eV) to the Si component. The simple spraying deposition method and the

wide variety of SWNT parameters (in terms of diameters, chirality and method of synthesis) provide sufficient benefits over DWNTs' less-explored nature as well as the lift-off deposition method [11, 12]. In addition, we show an important pre-spraying treatment of SWNTs that considerably improves the conversion efficiency, where the sediment fractions of the centrifuged SWNT suspension exhibit much better device performance than supernatant fractions. We explain this fact by the change of SWNT network morphology; the sediment contains longer and thicker SWNT bundles, resulting in higher conductivity than SWNT bundles from the supernatant.

2. Experimental details

For this study, purified semiconducting SWNTs (7,6 major chirality) obtained from SouthWest Nano Technologies, Inc were used. These nanotubes grown by the Co–Mo/SiO_2 method [13] were selected because of their semiconducting nature associated with a narrow chirality distribution [14]. SWNT films on Si and on glass substrates (as reference) were formed via spray coating from a nanotube suspension (0.5 mg ml^{-1}) in dichlorobenzene solution. Dichlorobenzene was used as a solvent because it gives the highest SWNT solubility attainable [15]. Prior to spraying, nanotubes were centrifuged (6500 rpm/5700g) for 30 min and the sediment collected after decantation was redispersed again by sonication in dichlorobenzene. Some samples were prepared without centrifugation (sonication for 30 min only). The solar cells were fabricated by spraying the SWNTs through a 5 mm × 5 mm window (active area) onto an n-type Si (100 orientation, $\rho = 0.01\ \Omega$ cm) surface that was previously cleaned and etched with hydrofluoric acid. A layer of Cr/Au (20/150 nm) was sputtered on the backside of the Si wafer to form an ohmic back contact with Si. The top contact to the SWNT film was made by a thin strip of silver paint (1 mm × 5 mm) over the SWNT film. The sheet resistance of all the fabricated solar cells was 1 kΩ/square, as measured from the glass reference sample during the spraying process.

The PV properties of the solar cells were tested under dark and illuminated conditions using a class-B solar simulator (PV Measurements, Inc.) at an irradiation intensity of 100 mW cm^{-2} (AM1.5 condition). I–V characteristics were detected using a Keithley 238 controlled by LabView software. NIR–vis absorption spectra were recorded with a Perkin Elmer Lambda 900 spectrometer. Photocurrent spectra measurements at zero bias were carried out using a Bruker Tensor 27 FTIR spectrometer equipped with an A/D converter module. The photocurrent signal after passing through a low noise preamplifier was digitized by the A/D converter and connected to the external interface of the FTIR spectrometer. Resonant Raman scattering was recorded using a Raman Systems R-3000 spectrometer with laser excitation of 500 mW at 785 nm. Scanning electron microscopy (SEM) images were taken with a Hitachi S-4300 microscope.

3. Results and discussion

Figure 1(a) shows the I–V characteristics of the SWNT/Si solar cells (prepared from sediment and supernatant) under dark and under light illumination. Short-circuit current density (J_{SC}), open-circuit voltage (V_{OC}), fill factor (FF) and conversion efficiency (η) are presented in table 1 for the non-centrifuged SWNT sample (sonication only) and after centrifugation for both the sediment and supernatant samples. Photocurrent density spectra of the solar cells in the NIR range and the corresponding absorption spectra of SWNTs sprayed on the glass (reference sample) are shown in figure 2. The photocurrent spectra were normalized to the device area and intensity of the Globar NIR/IR light source.

Table 1. Comparison of open-circuit voltage (V_{oc}), short-circuit current density (J_{sc}), fill factor (FF), conversion efficiency (η) and film transmittance (%) at 550 nm for non-centrifuged SWNTs (sonication only) and after centrifugation for both sediment and supernatant.

Sample	V_{oc} (V)	J_{sc} (mA cm^{-2})	FF	η (%)	% transmittance
Sediment (SD)	0.37	14.6	0.30	1.7	83
Supernatant (ST)	0.22	4.9	0.20	0.2	74
Sonication only	0.37	8.4	0.25	0.8	80

Comparison of the photocurrent with the NIR absorption spectra clearly indicates an excellent matching of the S_{11} band (corresponding to the first interband transition for SWNTs with 7,6 and 8,6 chirality) with the photocurrent band located at ∼1150 nm (figure 2). Thus, the SWNT film contributes to the photoconversion process not only as a charge separator/transporter/collector but also as a light absorber. This is an important fact, distinguishing between a heterojunction solar cell with two active light absorbing components and a Schottky cell, where the metal component is not capable of absorbing photons. To the best of our knowledge, no direct evidence of the SWNT contribution to photoconversion as light absorbers has been reported for the various SWNT-based solar cells [1–12].

As depicted in figures 1(a), (c) and (d) and listed in table 1, we found a striking difference in the conversion efficiency for the SWNT suspension sprayed from sediment (SD) and supernatant (ST) after centrifugation. SD-based cells demonstrate an efficiency (∼1.7%) higher by a factor of ∼8 as compared with ST cells (∼0.2%) and by a factor of two as compared with sonication only (∼0.8%) solar cells, where SWNTs were sprayed without centrifugation. The bulk conductivity of thick SD and ST films (20–30 μm) coated on glass was 9840 S m^{-1} and 760 S m^{-1}, respectively, as measured by the four-probe method. The higher conductivity of SD nanotubes compared to ST is also confirmed by the transmittance measurement at 550 nm as listed in table 1. At equal surface resistance, ST samples exhibit lower transmittance (∼74%) compared to SD samples (∼84%), which is indicative of the higher conductivity of the sediment content over the supernatant. The porosity of bulk sediment and bulk supernatant films is approximately 55% and 82%, respectively. The porosity of these films is calculated based on the ratio of the measured film mass over the mass of densely packed nanotube bundles in the same volume, taking into account the density of the pristine SWNT bundle is 1.87 g cm^{-3} [16]. SEM imaging of SD-and ST-based

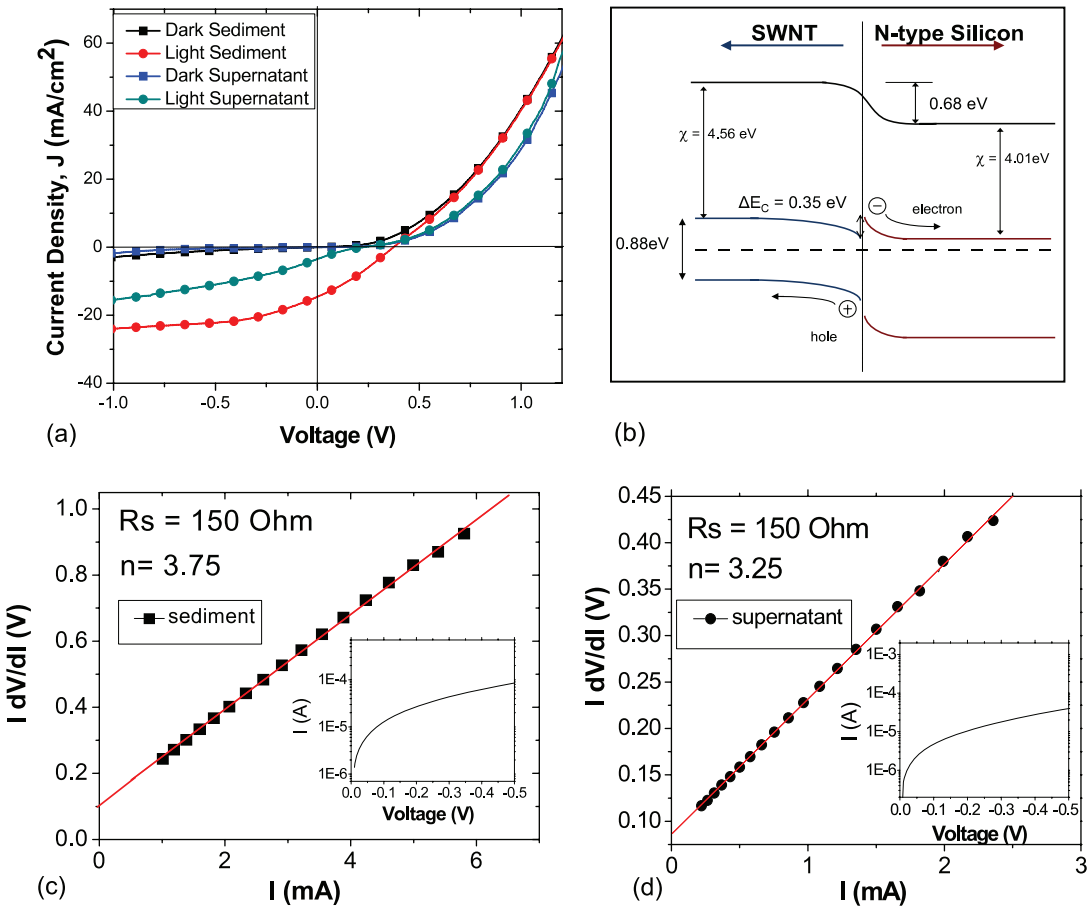

Figure 1. (a) Current–voltage (J–V) plot of sediment and supernatant SWNT/n-Si devices under dark and light illumination. (b) Schematic energy band diagram of SWNT-n-Si heterojunction based on the Anderson model. Electron affinity χ and conduction band offset ΔE_c for SWNTs and n-Si are shown in the energy band diagram. Line plot of $I(\mathrm{d}V/\mathrm{d}I)$ against I, where the slope corresponds to the series resistance of (c) sediment and (d) supernatant samples. The inset of (c) and (d) shows the dark I–V of the sediment and supernatant samples, respectively, in reverse bias, where the slope corresponds to the shunt resistance.

solar cells (figures 3(a)–(d)) reveals different morphologies for the corresponding SWNT films. For the sediment samples, nanotube bundles are thicker (average diameter ∼26 nm, figure 3(e)) and longer compared with supernatant bundles (average diameter of ∼19 nm, figure 3(f)). The high speed centrifugation process separates the higher density nanotube bundles (sediment) from the less dense nanotube bundles (supernatant). Thus, the higher density nanotube bundles in the sediment fraction contain more nanotubes than the supernatant, which explains the thicker distribution of nanotube bundles in the sediment samples. In addition, the SWNT porous film for SD has larger openings so that the silicon surface is exposed (figure 3(a)). In contrast, the SWNT film for ST is denser and covers the entire Si surface (figure 3(b)). An enhanced SD conductivity can be rationalized in terms of the morphology of the SWNT network. As was demonstrated previously [17], the resistance of an SWNT network is mostly defined by the junction between bundles, not by the resistance of the bundles alone. The longer bundles should decrease the number of junctions in the nanotube network and thicker bundles should increase the junction cross-sectional area, resulting in reduced resistance of the junction. This explanation is fully consistent with the SEM images and the conductivity measurements. Thus, the poor efficiency of the ST solar cell can be explained by (i) higher SWNT film resistivity due to thin and short bundles as compared with the SD-based cell and (ii) a thick and low porosity film absorbing most of the incident light and blocking it from the Si. Centrifugation is widely used for CNT purification to remove amorphous carbon and catalysts [18–20]. Low speed centrifugation (∼3000 g) was shown to remove amorphous carbon, resulting in higher purity of the sediment [19] and, conversely, high speed centrifugation (20 000g) is effective in sedimenting carbon nanoparticles leaving the ST fraction more conductive and of higher purity [20]. In both previous cases, the relative purity measured by NIR absorbance [21] was different for the SD and ST fractions. However, in our experiment, the relative purity for both the SD and ST fractions based on the NIR absorbance method [21] is similar (NIR absorbance spectra of SWNTs in dichlorobenzene are not shown here). Further, the Raman

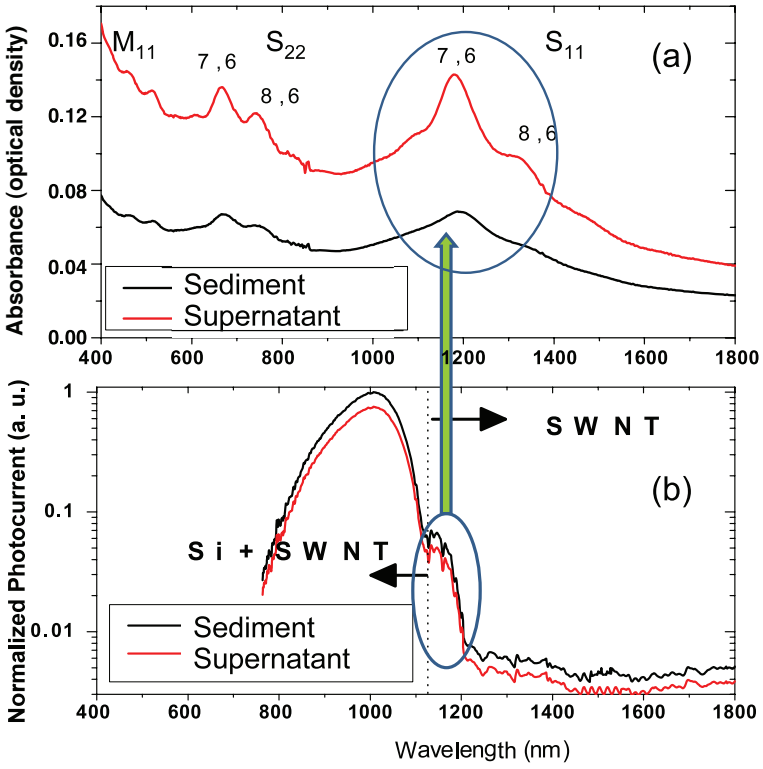

Figure 2. (a) UV–vis NIR spectrum of sediment and supernatant fraction from the centrifugation process of SWNT films on glass with sheet resistance of 1 kΩ/square. M_{11}, S_{22} and S_{11} represent the bandgap transitions in metallic and semiconducting SWNTs. (b) Normalized photocurrent spectra (area and intensity of light source) of the solar cell devices (supernatant and sediment) showing a current peak band (due to SWNTs) matching the S_{11} band.

spectra (figure 4) indicate that the ST and SD samples exhibit the same SWNT purity, where the ratio of G (tangential mode at 1590 cm^{-1}) and D (disorder-induced mode at 1292 cm^{-1}) bands are similar. The G/D ratio is widely used as a criterion of carbon nanotube purity [22]. A possible explanation could be that the initial high purity (more than 95%) of 7,6 SWNTs is higher than the as-prepared arc discharge SWNTs with HNO_3 treatment [18, 19]. Thus, in our case, the centrifugation process does not significantly affect the relative purity of the SWNTs, but simply causes the separation of the high (SD) and low (ST) conductive fractions.

Careful examinations of the Raman spectra (figure 4) reveal differences in the shape of the G band for both the sediment and supernatant samples. Deconvolution of the G band (figures 4(b) and (c)) on the two sub-bands (G^- and G^+) using the asymmetric Breit–Wigner–Fano (BWF) shape (G^-) and Lorentzian shape (G^+) results in a different ratio of G^-/G^+. For SD this value is 0.167 as compared to 0.12 for ST. The BWF shape of the G^- sub-band is usually attributed to the presence of metallic nanotubes [23]. Although the mass of metallic SWNTs should be significantly smaller than semiconducting 7,6 nanotubes, their contribution to the sediment fraction could be increased non-proportionally after centrifugation as compared with the supernatant (e.g. two bands in the absorbance spectrum in the range of 400–550 nm (figure 2) could be assigned to metallic SWNTs). Presumably this can be associated with the different surface charges for metallic and semiconducting nanotubes (and bundles of different natures), resulting in their separation. The presence of metallic nanotubes/bundles should improve the charge transport and collection due to their high conductivity, while semiconducting nanotubes mostly contribute to only light absorbance and charge separation at the Si interface.

The band diagram for the SWNT/Si heterojunction is illustrated in figure 1(b) based on the Anderson model [24], despite the limitations associated with the one-dimensional nature of carbon nanotubes. The devices exhibit a typical p–n junction current rectification behavior which is consistent with the high conduction band offset of 0.35 eV and built-in potential of 0.68 eV based on the following parameters. The SWNT conduction band (E_c) is 4.36 eV based on a work function of 4.8 eV [25], a calculated bandgap of 0.88 eV ($E_G = (2 \times \gamma \times a_{c-c})/d_t$ [26], where the diameter d_t of 7,6 SWNTs is 0.9 nm, γ is 2.77 eV and the π–π energy overlap between neighboring atoms a_{c-c} is 0.1421 nm, the nearest-neighbor distance between carbon atoms) and the Fermi level in the middle of the bandgap. In addition, the rectifying behavior at forward bias (applied to the SWNT side) is also similar to the data observed elsewhere [10–12, 27, 28]. Control samples made of graphite powder deposited on the Si substrate (prepared and sprayed in the same way as SWNTs) and bare Si with only a silver paint strip did not exhibit any photovoltaic effects.

The shunt resistance which is obtained from the slope of the reverse current in the range of 0.2–0.4 V is approximately

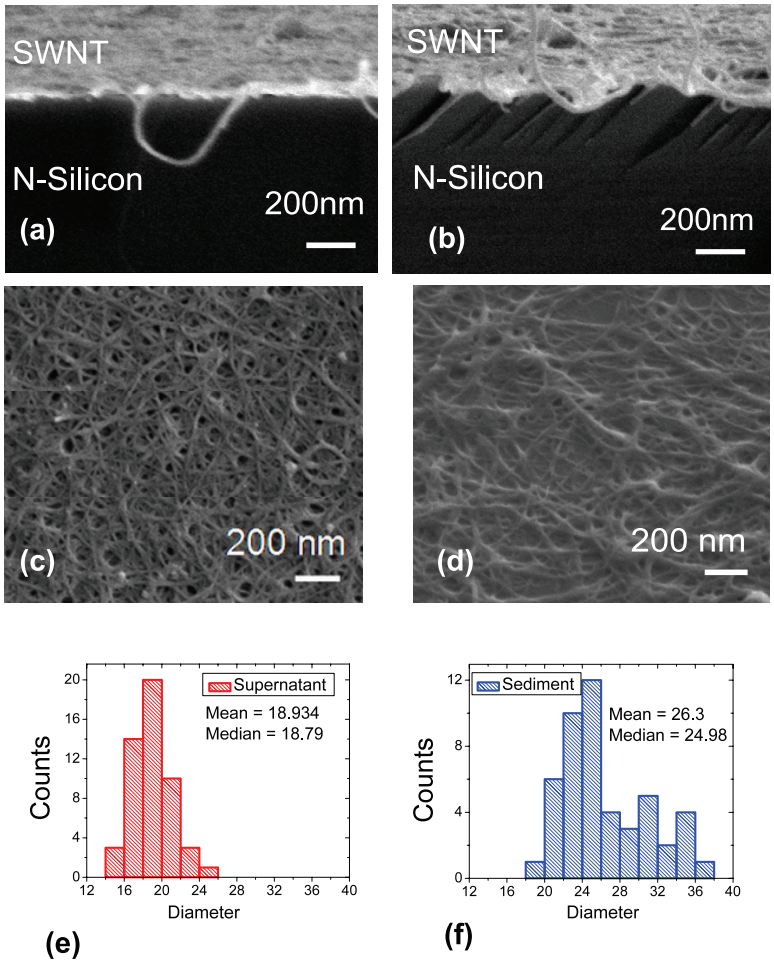

Figure 3. SEM images of (a) cross-sectional view of supernatant, (b) cross-sectional view of sediment, (c) top view of supernatant and (d) top view of sediment. Diameter distribution histogram of SWNT bundles (50 samples) for (e) supernatant and (f) sediment. From the SEM images and histogram, the sediment sample shows thicker and longer SWNT bundles compared to the supernatant.

7 kΩ and 10 kΩ for the sediment and supernatant samples, respectively (inset of figures 1(c) and (d)). Calculations of series resistance R_S result in approximately the same values of ∼150 Ω for sediment and supernatant samples. However, the ideality factor for ST was lower (3.25) than for SD (3.75). The major contributions of R_S come from the sheet resistance of the SWNT film, the interface resistance between the SWNT film and the Si substrate, and the contact resistance between SWNTs and the silver paint. Although the sheet resistance of the sediment film is lower than the supernatant film, the other contributions (contact and interface resistance) dominate over the SWNT sheet resistance. Thus, the total series resistance for SD and ST are similar. Presumably, the contact resistance provides the major contribution to the series resistance. Then, an improvement of the top contact by metal grid deposition should result in better PV performance. The R_S values were obtained from the slope of a line of the plot (figures 1(c) and (d)) of $I(\mathrm{d}V/\mathrm{d}I)$ against I in the 0.2–0.9 V region based on the equation [29]

$$I\frac{\mathrm{d}V}{\mathrm{d}I} = R_s I + \frac{n_2 kT}{q} \tag{1}$$

where k, T and q are Boltzmann's constant, temperature and elementary charge, respectively.

The ideality factor, n_2, was obtained from fitting our experimental I–V curves to the diode equation (equation (2)) and the extrapolation to the zero crossing of the $I(\mathrm{d}V/\mathrm{d}I)$ axis in the line plot of figures 1(c) and (d):

$$I = I_1 \exp\left(\frac{qV}{n_1 kT}\right) + I_2 \exp\left(\frac{qV}{n_2 kT}\right). \tag{2}$$

Although the diode ideality factors are relatively high, these values are comparable to heterojunction solar cells based on electrodeposited CdTe/CdS films [27]. Despite the lower ideality factor and the equal series resistance of the ST-based cell compared to the SD-based cell, the low conversion efficiency of the ST-based cell can be explained by the 'kink behavior' (shown in the I–V curves, figure 1), which decreases the V_{oc} and I_{sc} values. A similar 'kink' was also observed in other reports [30, 31] and was explained in a theoretical study [32]. Charge transport in the SWNT network is usually characterized by Mott's variable range hopping (VRH) mechanism [33]. Thus, it is reasonable to suggest that, in

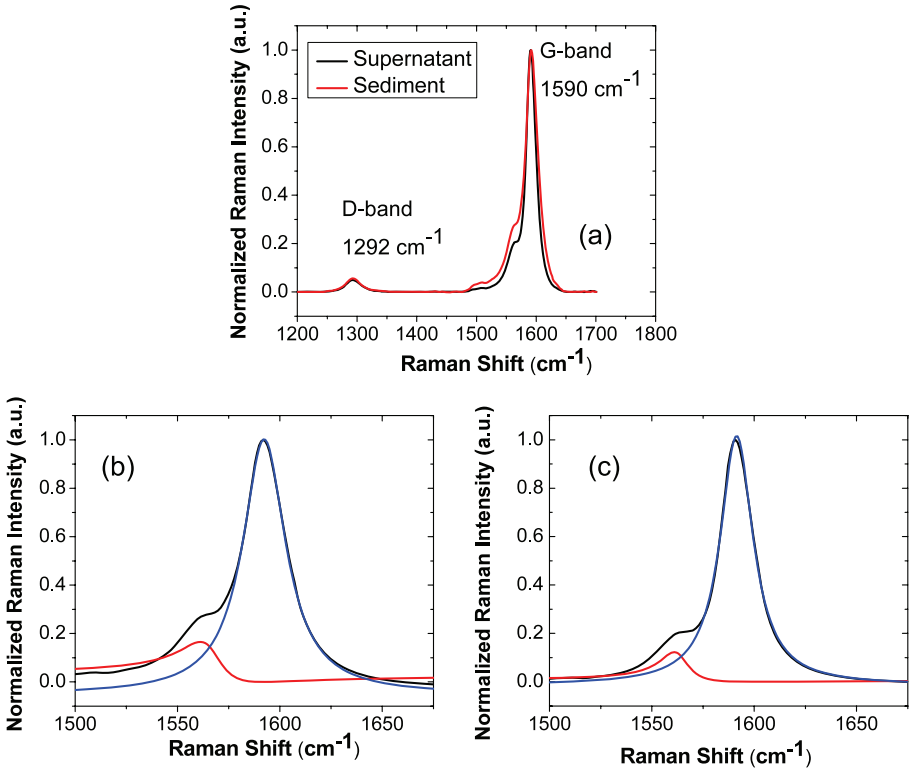

Figure 4. (a) Normalized (on the maximum G band) Raman spectra of supernatant and sediment SWNT films on the n-Si substrate. Deconvolution of the G band (experimental data, black line) for (b) sediment and (c) supernatant samples, using the asymmetric Breit–Wigner–Fano (BWF) lineshape function (G^- band, red line) and Lorentzian function (G^+ band, blue line).

low conductive ST film, the hopping probability is reduced due to higher charge localization at the junction sites between bundles. This is consistent with the theoretical model [32], indicating that the I–V curve degradation ('kink' feature) occurs as a result of a decrease of the hopping rate.

4. Conclusions

In conclusion, we demonstrate that the SWNT network can be used in conjunction with n-Si to form a heterojunction solar cell. Distinct from previous studies [10–12], we have shown for the first time that SWNTs absorb incident light and directly contribute to the photoconversion process. Thus, SWNTs serve as active photosensing material involving not only charge separation, transport and collection but also light absorption. The parameters of the photovoltaic devices in this study were not optimized, therefore there is substantial potential for the following performance improvements such as (i) SWNT doping to increase nanotube conductivity, (ii) selection of an optimal film thicknesses to provide a balance between Si and SWNT absorption, (iii) multi-step centrifugation to refine further the network morphology, (iv) the use of porous Si to reduce the reflection from the Si surface or (v) increasing n-Si doping. Finally, improving the top contact by reducing the series resistance (e.g. metal grid deposition instead of a silver paint strip) should substantially increase the conversion efficiency. The simple and scalable SWNT wet deposition offers to create a variety of p–n junctions with other n-type substrates other than crystalline Si, e.g. any crystalline thin film amorphous/nanoporous semiconductors. In addition, the spray coating technique can also be incorporated for flexible solar cells by spraying the nanotube films on any flexible substrate materials (i.e. metal foil/polyimide) with prior deposition of thin film amorphous Si. Indeed, the non-optimized solar cell devices in this study exhibit a conversion efficiency ∼2% which is higher than any polymer–carbon nanotube devices developed so far [1–7]. Such hybrid cells can be considered as a promising alternative to the widely studied CNT–polymer composites for thin film photovoltaics.

Acknowledgments

This work is supported by a US Army grant. We thank Dr Song Youngsik for the SEM images.

References

[1] Geng J and Zeng T 2006 *J. Am. Chem. Soc.* **128** 16827
[2] Pradhan B, Batabyal S K and Pal A J 2006 *Appl. Phys. Lett.* **88** 093106
[3] Landi B J, Raffaelle R P, Castro S L and Bailey S G 2005 *Prog. Photovolt., Res. Appl.* **13** 165
[4] Ago H, Petritsch K, Shaffer M S P, Windle A H and Friend R H 1999 *Adv. Mater.* **11** 1281

[5] Kymakis E and Amaratunga G A 2002 *J. Appl. Phys. Lett.* **80** 112
[6] Bhattacharyya S, Kymakis E and Amaratunga G A 2004 *Chem. Mater.* **16** 4819
[7] Kymakis E, Koudoumas E, Franghiadakis I and Amaratunga G A 2006 *J. Phys. D: Appl. Phys.* **39** 1058
[8] W Rowell M, Topinka M A, McGehee M D, Prall H J, Dennler G, Sariciftci N S, Hu L and Gruner G 2006 *Appl. Phys. Lett.* **88** 233506
[9] van de Lagemaat J, Barnes T M, Rumbles G, Shaheen S E, Coutts T J, Weeks C, Levitsky I, Peltola J and Glatkowski P 2006 *Appl. Phys. Lett.* **88** 233503
[10] Li Z, Kunets V P, Saini V, Xu Y, Dervishi E, Salamo G J, Biris A R and Biris A S 2008 *Appl. Phys. Lett.* **93** 243117
[11] Jia Y *et al* 2008 *Adv. Mater.* **20** 4594
[12] Wei J *et al* 2007 *Nano Lett.* **7** 2317
[13] Alverez W E, Pompeo F J, Herrera E, Balzano L and Resasco D E 2002 *Chem. Mater.* **14** 1853
[14] Bachilo S M, Balzano L, Herrera J E, Pampeo F, Resasco D E and Weisman R B 2003 *J. Am. Chem. Soc.* **125** 11186
[15] Bahr J L, Mickelson E T, Bronikowski M J, Smalley R E and Tour J M 2001 *Chem. Commun.* **2** 193
[16] Lu Q, Keskar G, Ciocan R, Rao R, Mathur R B, Rao A M and Larcom L L 2006 *J. Phys. Chem.* B **110** 24371
[17] Stadermann M *et al* 2004 *Phys. Rev.* B **69** 201402
[18] Dujardin E, Ebbesen T W, Krishnan A and Treacy M J 1998 *Adv. Mater.* **10** 611
[19] Hu H, Yu A, Kim E, Zhao B, Itkis M E, Bekyarova E and Haddon R C 2005 *J. Phys. Chem.* B **109** 11520
[20] Yu A, Bekyarova E, Itkis M E, Fakhrutdinov D, Webster R and Haddon R C 2006 *J. Am. Chem. Soc.* **128** 9902
[21] Itkis M E, Perea D E, Jung R, Niyogi S and Haddon R C 2005 *J. Am. Chem. Soc.* **127** 3439
[22] Dillon A C, Gennett T, Jones K M, Alleman J L, Parilla P A and Heben M J 1999 *Adv. Mater.* **11** 1354
[23] Brown S D M, Jorio A, Corio P, Dresselhaus M S, Dresselhaus G, Saito R and Kneipp K 2001 *Phys. Rev.* B **63** 155414
[24] Davies J H 1998 *The Physics of Low-Dimensional Semiconductors* (Cambridge: Cambridge University Press)
[25] Zhao J, Han J and Lu J P 2002 *Phys. Rev.* B **65** 193401
[26] Mintmire J W and White C T 1995 *Carbon* **33** 893
[27] Hu J, Ouyang M, Yang P and Lieber C M 1999 *Nature* **399** 48
[28] Tzolov M, Chang B, Yin A, Straus D, Xu J M and Brown G 2004 *Phys. Rev. Lett.* **92** 075505
[29] Rakhshani A E 2001 *J. Appl. Phys.* **90** 4265
[30] Peumans P and Forrest S R 2001 *Appl. Phys. Lett.* **79** 126
[31] Levitsky I A, Euler W B, Tokranova N, Xu B and Castracane G 2004 *Appl. Phys. Lett.* **85** 6245
[32] Nelson J, Kirkpatrick J and Ravirajan P 2004 *Phys. Rev.* B **69** 035337
[33] Mott N F and Davis E A 1971 *Electronic Process in Non-Crystalline Solids* 1st edn (London: Oxford University Press)